Int. J. Dev. Biol. **ACCEPTED MANUSCRIPT**
https://doi.org/10.1387/ijdb.200173lv

THE INTERNATIONAL JOURNAL OF DEVELOPMENTAL BIOLOGY
www.intjdevbiol.com

Developmental delay during eye morphogenesis underlies optic cup and neurogenesis defects in *mab21l2*^{u517} zebrafish mutants

REBECCA WYCLIFFE, JULIE PLAISANCIE, SYDNEY LEAMAN, OCTAVIA SANTIS, LISA TUCKER, DANIELA CAVIERES, MICHELLE FERNANDEZ, CAMILA WEISS-GARRIDO, CRISTIAN SOBARZO, GAIA GESTRI and LEONARDO E. VALDIVIA

Developmental delay during eye morphogenesis underlies optic cup and neurogenesis defects in *mab21l2*^{u517} zebrafish mutants

Rebecca Wycliffe[1], Julie Plaisancie[2,3], Sydney Leaman[1], Octavia Santis[4], Lisa Tucker[1], Daniela Cavieres[4], Michelle Fernandez[4], Camila Weiss-Garrido[4], Cristian Sobarzo[4,5], Gaia Gestri[1], Leonardo E. Valdivia[4,5]*

[1] Department of Cell and Developmental Biology, University College London, London, United Kingdom
[2] UDEAR, UMR 1056 Inserm-Université de Toulouse, Toulouse, France.
[3] Department of Medical Genetics, CHU Toulouse, Toulouse, France.
[4] Center for Integrative Biology, Facultad de Ciencias, Universidad Mayor, Santiago, Chile.
[5] Escuela de Biotecnología, Facultad de Ciencias, Universidad Mayor, Santiago, Chile.

*Corresponding author

Contact details:

Leonardo Esteban Valdivia, Ph.D.

Assistant Professor

Center for Integrative Biology
Facultad de Ciencias
Universidad Mayor
Camino La Piramide 5750
Huechuraba
Santiago
Chile

Phone: +56225189239
leonardo.valdivia@umayor.cl

Short running title: **Developmental delay in *mab21l2* mutant eyes**

Abbreviations

-CMZ: ciliary marginal zone
-hpf: hours post fertilization
-RPC: Retinal Progenitor Cell
-*mab21l2*: *male abnormal 21-like 2*
-*vsx2*: *visual homeobox 2*

Abstract

Background: Shaping the vertebrate eye requires evagination of the optic vesicles. These vesicles subsequently fold into optic cups prior to undergoing neurogenesis and allocating a population of late progenitors at the margin of the eye. *mab21l2* encodes a protein of unknown biological function expressed in the developing optic vesicles, and loss of *mab21l2* function results in malformed eyes. The bases of these defects are, however, poorly understood. **Methods:** To further study *mab21l2* we used CRISPR/Cas9 to generate a new zebrafish mutant allele (*mab21l2*^{u517}). We characterized eye morphogenesis and neurogenesis upon loss of *mab21l2* function using tissue/cell-type-specific transgenes and immunostaining, *in situ* hybridization and bromodeoxyuridine incorporation. **Results:** *mab21l2*^{u517} eyes fail to grow properly and display an excess of progenitors in the ciliary marginal zone. The expression of a transgene reporter for the *vsx2* gene –a conserved marker for retinal progenitors– was delayed in mutant eyes and accompanied by disruptions in the epithelial folding that fuels optic cup morphogenesis. Mutants also displayed nasal-temporal malformations suggesting asynchronous development along that axis. Consistently, nasal retinal neurogenesis initiated but did not propagate in a timely fashion to the temporal retina. Later in development, mutant retinas did laminate and differentiate. Thus, *mab21l2*^{u517} mutants present a complex eye morphogenesis phenotype characterized by an organ-specific developmental delay. **Conclusions:** We propose that *mab21l2* facilitates optic cup development with consequences both for timely neurogenesis and allocation of progenitors to the zebrafish ciliary marginal zone. These results confirm and extend previous analyses supporting the role of *mab21l2* in coordinating morphogenesis and differentiation in developing eyes.

Keywords: eye, *mab21l2,* morphogenesis, differentiation, zebrafish, microphthalmia

Introduction

Development of vertebrate eyes begins with specification of the eyefield as a single domain within the anterior neural plate (Bazin-Lopez *et al.*, 2015; Cavodeassi and Houart, 2012)Subsequently, cells destined to form left and right eyes evaginate laterally splitting the eyefield into two optic vesicles that undergo further morphogenesis (Bazin-Lopez *et al.*, 2015; Ivanovitch *et al.*, 2013; Martinez-Morales *et al.*, 2009). Orchestration of cell proliferation, dynamic modifications in cell shape and cell polarity, and precisely coordinated cell movements, culminate in the formation of the optic cups (Fuhrmann, 2010). At this developmental timepoint, multipotent retinal progenitors acquire post mitotic fates sequentially in a conserved order of differentiation (Chow and Lang, 2001; Fuhrmann, 2010)

The description of eye morphogenesis and differentiation has been highly refined over the last years. This is in part due to advances in imaging techniques using translucent zebrafish and medaka fish embryos. These models have been pivotal to get a better grasp of the complex cell choreography that transforms optic vesicles into cups and beyond (Heermann *et al.*, 2015; Kwan *et al.*, 2012; Martinez-Morales *et al.*, 2009; Picker *et al.*, 2009) In zebrafish, studies of this morphogenesis have identified several cellular behaviours including cell flattening, basal constriction of retinal cells' end-feet, and a process named “epithelial flow”. In epithelial flow, cells contribute to eye growth by moving collectively around the rims of the folding optic cup in a process that is facilitated by a tight modulation of BMP signalling (Heermann *et al.*, 2015; Martinez-Morales *et al.*, 2017; Picker *et al.*, 2009)

Shaping of the eye coincides with a gradual restriction in cell fate. Maturation of the optic cups requires both proliferation and differentiation of retinal progenitor cells (RPCs) to produce neurons and glia. In zebrafish, neurogenesis begins with the circumferential propagation of a differentiation wave arising from the ventronasal retina at approximately 28 hours post fertilization (hpf). This is preceded by comparable waves of expression of neurogenesis-related genes such as *atoh7* (Masai *et al.*, 2000; Poggi *et al.*, 2005). By 60hpf, neurogenesis occurs almost exclusively from a peripheral area of the retina named the ciliary marginal zone (CMZ), which contains a true stem cell niche that fuels both the growth of the retina and persistent differentiation throughout life (Centanin *et al.*, 2011; Stenkamp, 2007). Epithelial flow is important for allocating cells to the CMZ, which is consistent with the expression of genes that are initially found in the whole early eye and subsequently confined to the CMZ, such as the conserved retinal progenitor marker *vsx2* (Reinhardt *et al.*, 2015; Vitorino *et al.*, 2009). Successful morphogenesis is important both to the maturation of the optic cup and correct progenitor allocation in developing eyes.

Mutations in critical genes for eye development result in ocular malformations. Among the genes causing arrest in growth of the eyes (microphthalmia) in humans, those encoding transcription factors represent the largest group. Mutations in the HMG-box gene *SOX2* is the most common genetic cause, followed by mutations in homeodomain-containing factor-encoding genes *RAX, PAX6*, members of the *SIX* family, and the *VSX2* gene; all these genes are required for eye progenitor competence and cell survival (Fantes *et al.*, 2003; Gerth-Kahlert *et al.*, 2013; Reis and Semina, 2015). Members of the TGF-β/BMP family (including *BMP4*, *BMP7* and *GDF6*), and other isolated genes (*C12orf57*, *TENM3, PXDN, YAP*) also cause microphthalmia when mutated (Reis and Semina, 2015). More recently, mutations in *MAB21L2* –a gene encoding a protein of largely unknown function– were shown to result in a range of eye malformations including microphthalmia (Deml *et al.*, 2015; Rainger *et al.*, 2014). Understanding the function of poorly studied genes such as

mab21l2 is important to expand our knowledge on the gene networks that sculpt eye development.

Mab21l2 is a highly conserved gene. It was named after the ortholog *male-abnormal 21* (*mab-21*) in *C. elegans* where it was first characterized (Chow and Emmons, 1994). Two *mab21-like* orthologues are present in vertebrates, named *Mab21l1* and *Mab21l2*, which are similar in DNA sequence and expressed in extensive overlapping domains during eye formation suggesting redundant functions (Kudoh and Dawid, 2001; Wong *et al.*, 1999). *Mab21l2* has been more studied because of its association to human disease (Deml *et al.*, 2015; Kudoh and Dawid, 2001; Mariani *et al.*, 1998; RLY Wong and Chow, 2002). In mouse, chicken and frog, *mab21l2* is expressed in developing eyes; in zebrafish, *mab21l2* is expressed in optic vesicles, optic cups and CMZ, as well as in subsets of retinal neurons (Deml *et al.*, 2015; Kudoh and Dawid, 2001; YM Wong and Chow, 2002).

The function of *mab21l2* is also highly conserved. *MAB21L2* mutations in human result in microphthalmia (Rainger *et al.*, 2014). Loss of Mab21l2 in mice result in microphthalmic malformed retinas linked to proliferative deficits (Tsang *et al.*, 2018; Yamada *et al.*, 2004). *MAB21l2* knockdown at optic cup stages in chick embryos affects neuronal differentiation in the retina (Sghari and Gunhaga, 2018), suggesting that *Mab21l2* has diverse roles during vertebrate eye formation. Zebrafish models have been used to test causality of human mutations, as well as for phenotyping; defects in mutant eyes include lens, cornea and vascular malformations, and increased levels of cell death (Deml *et al.*, 2015; Gath and Gross, 2019; Hartsock *et al.*, 2014; Kennedy *et al.*, 2004). Regardless the conserved role of *mab21l2* during eye development, we do not fully understand how *mab21l2* influences shaping of the optic cup (Gath and Gross, 2019; Hartsock *et al.*, 2014). The morphogenetic processes driven by *mab21l2* have been poorly characterised in whole eyes, which is a necessary step to inform disease mechanisms and function of the Mab21l2 protein during ocular development.

Overall, the whole transformation from vesicles to cups involves cell shape changes and collective cell movements that set the stage for subsequent eye development. Studying the function of poorly studied genes such as *mab21l2* is essential to get a better overview of the genetics underlying eye formation. Here, we generated a new loss of function zebrafish allele, confirmed previous analyses (Deml *et al.*, 2015; Gath and Gross, 2019) and describe novel aspects of the *mab21l2* role. Mutant eyes fail to grow properly. Counterintuitively, these small eyes apparently have more proliferative progenitors in the CMZ. The absence of functional Mab21l2 delays the expression of a reporter for *vsx2*, which is an evolutionarily conserved microphthalmia-causing gene, and is accompanied with profound optic cup folding defects. Uncoupling nasal and temporal development of the retina in mutants, correlates with a delay in the propagation of neurogenesis across the axis of the eye. Overall, we describe the *mab21l2* mutant phenotype at defined time points of eye development and show that *mab21l2* is required for successful morphogenesis of the optic cup. Such events have consequences both for the timing of the transition from proliferation to differentiation in the embryonic retina and for the establishment of the CMZ.

Materials and methods

Zebrafish husbandry

Embryos were obtained using natural spawning and raised at 28.5°C. Staging was performed according to standard criteria (Kimmel *et al.*, 1995). Embryos were kept in petri dishes containing fish system water supplemented with methylene blue (2 ml of 0.1% methylene blue in 1 litre of system-water). For *in situ* hybridisation and immunofluorescence experiments, 1-phenyl 2-thiourea (PTU) (Sigma) was added before 24 hours post fertilization (hpf) at a final concentration of 0.003% to prevent pigmentation. Embryo fixation was carried out in 4% paraformaldehyde (PFA) in phosphate buffered saline solution (PBS).

Heterozygote *mab21l2* mutant carriers were crossed to either *tg(vsx2:GFP)*^{nns1} (Kimura *et al.*, 2006) or *tg(atoh7:GAP-mRFP)*^{cu2} (Zolessi et al, 2006), to obtain double carriers. For all experiments we used a single copy of the transgenes.

Generation of a zebrafish mab21l2 mutant

We used CRISPR/Cas9 for editing the zebrafish *mab21l2* locus and established the *mab21l2*^{u517} line. The CRISPR design tool (http://zifit.partners.org/ZiFiT/) was used to identify a target region in the single exon of the *mab21l2* gene. A DNA fragment of 117 base-pair (bp) harbouring a T7 promoter positioned upstream of a gRNA sequence bearing customized 20 nucleotides targeting sequences (GGTGTCGGATGTGCTGAAGG) was constructed by commercial DNA synthesis (GeneArt, Thermo Fisher) using the sequence template (from Hwang et al, 2013). The gRNA was generated using the HiScribe T7 High Yield RNA Synthesis Kit (NEB) followed by DNase I (NEB) digestion and purification with RNeasy MiniKit (Qiagen). The Cas9-encoding plasmid pT3TS-nCas9n (Addgene) (Jao et al, 2013) was linearized with XbaI (NEB) and capped mRNA synthesized with the mMessage mMachine T3 Transcription Kit (Thermo Fisher) followed by polyadenylation using the Poly(A) Tailing Kit (Thermo Fisher). The synthesised mRNA was purified using the RNeasy Mini Kit. Cas9 mRNA and gRNA were co-injected into one-cell stage AB wildtype embryos at 150 picograms and 30 picograms per specimen, respectively. At 24 hpf, embryos were assayed for targeted mutations using High Resolution Melting Analysis (HRMA) after genomic DNA extraction.

High-resolution melting analysis

Genomic DNA extraction was carried out using the HotShot Method (Meeker *et al.*, 2007). Briefly, lysis of single embryos (24 hpf) or fin clips from adult zebrafish were done by incubating the tissue in 25 or 50 µl base solution (1.25 M KOH and 10 mM EDTA), respectively, at 95 °C for 30 min followed by addition of 25 or 50 µl neutralization solution (2 M Tris HCL). HRMA analysis (Dahlem et al, 2012) was used to assess the mutagenesis rate in F0 and F1 embryos using the Precision Melt Supermix (Bio-Rad) on a CFX96 Touch Real-Time Thermocycler (Bio-Rad) according to the manufacturer's instructions. Primers used for HRMA were *Forward* 5'-CCATCGCCAAGACCATACGA-3' and *Reverse* 5'- GATGAAACGGGGCTCTTGGA-3'. Resulting data were analysed with Bio-Rad Precision Melt Analysis software by comparing melt curves from injected zebrafish with uninjected wild type. To know the molecular nature of the mutations introduced, a region of 424 base pairs around the gRNA target site was PCR-amplified using Taq DNA polymerase (Thermo fisher) using primers *mab21l2_4_F2_seq* 5'-GGAGTTGTGCCTCTGGCTTC-3' and *mab21l2_4_R2_seq* 5'-ACCGGAACAGACCATCAGTT-3', and sequenced using the *mab21l2_4_F2_seq* primer.

Genotyping

To identify the genotype of *mab21l2*^{u517} carrier fish, as well as the offspring from an incross of heterozygous carriers, we used the Kompetitive Allele Specific PCR genotyping assay (KASP, LGC Genomics). For each KASP reaction, 0.11 ul of the *mab21l2*^{u517} primer assay (LGC assay number 1113070274), 4 µl (2X) KASP buffer mix, 1 µl Nuclease-free water and 1 µl DNA were used. The PCR program was set according to the manufacturer's instructions. Embryos were separated according to homozygous mutants or siblings, as carriers for *mab21l2*^{u517} have no phenotype. For histological analyses, homozygous mutants and sibling embryos were used.

RNA extraction and quantitative real-time PCR

Total RNA was extracted from tissues or pools of 25 zebrafish embryos at 14 somite stage, using the TRIzol protocol (Thermo Fisher). Complementary DNA was synthetized with a SuperScript III First Strand Reverse Transcriptase (Thermo Fisher) using 1 µg of total RNA per reaction. Quantitect primers (Qiagen) were used to amplify *mab21l2* (QT02206792) and β-actin (QT02174907). Real-time PCR was performed on a CFX96 Touch Real-Time Thermocycler (Bio-Rad) using a GoTaq qPCR Master Mix (Promega). Fold change in transcript levels was calculated using the ΔΔCt method normalising to β-actin levels (Livak and Schmittgen, 2001).

Bromodeoxyuridine incorporation

Incorporation of Bromodeoxyuridine (BrdU) was carried out at room temperature as previously described (Valdivia et al, 2016). Briefly, 1 nanoliter pulses of 10 mg/ml BrdU in fish water were injected into the hearts of 54 hpf embryos anaesthetised with MS-222 and immobilised in 1% low melting point agarose dissolved in fish water. After injection, embryos were removed from agarose and incubated at 28.5 °C in fish water with methylene blue until fixation with 4% paraformaldehyde.

In situ hybridization

To prepare *in situ* hybridization probes, DNA templates were obtained by linearization of plasmids containing *atoh7* and *ccnd1* cDNAs using the EcoRI and NotI restriction enzymes, respectively. RNA probes were synthesised by *in vitro* transcription. Appropriate polymerases (T7, T3; Promega) and digoxigenin-labelled nucleotides (Roche) were used for the synthesis of antisense RNAs according to manufacturer's instructions. Synthesized probes were purified using RNAeasy kit (Qiagen). Embryos were fixed and processed as previously described (Thisse and Thisse, 2008) and hybridization signals were detected using anti-digoxigenin-AP antibody (1:4000; 11093274910, Roche) and the NBT/BCIP chromogenic substrate (1:3.5; Roche). After the procedure, embryos were fixed and stored at 4°C until imaging

Immunohistochemistry

For whole-mount immunofluorescence, embryos were fixed in 4% PFA and kept at 4°C overnight. Samples were processed according to Valdivia et al, 2016. For sectioning, after fixation embryos were cryoprotected by sequential incubation in 15% and 30% sucrose dissolved in PBS for 12-16 h at 4°C. They were embedded in OCT resin, frozen on dry ice, and sectioned at 16 µm using a Leica cryostat. All immunostaining steps were performed at room temperature (~22°C).

The primary antibodies used were: chicken anti-GFP (ab13970, Abcam; 1:1000); rabbit anti-RFP (PM005, Medical & Biological Laboratories Co.; 1:2500); mouse anti-BrdU (3262F, Millipore; 1:200); rabbit anti-PH3 (06-570, Millipore; 1:400); mouse-anti Acetylated Tubulin (T7451, Sigma; 1:1000); mouse-anti HuC/D (A-21271, Molecular probes: 1:200). Secondary antibodies were anti-Chicken Alexa-488 (Thermo Fisher), anti-mouse Alexa 568 (Thermo Fisher) and anti-rabbit Alexa 568 (Thermo Fisher).

Microscopy and image analyses

After *in situ* hybridisation or before immunostaining, embryo tails were genotyped and heads and/or dissected eyes were either imaged using a Nikon E1000 microscope equipped with DIC 20×0.5 NA and 40×1.15 NA objective lenses, or subjected to immunohistochemistry. After immunohistochemistry, sections or agarose-embedded embryos were imaged with a Leica SPE8 (25×0.95 NA and 40×0.8 NA water immersion objectives) confocal microscope.

Images were processed using FIJI and/or Imaris (Bitplane) software. For quantifying PH3+ cells, images were blind-counted using ImageJ. For eye and section size measurements, images taken from a lateral view at fixed magnification were opened in ImageJ. The freehand selection tool was used to select to outline and calculate the area of each eye. Data were exported to Prism (GraphPad) for statistical analysis and graphing.

Results

mab21l2^{u517} mutants have small eyes and expanded ciliary marginal zone

Several *mab21l2* mutants have been identified in zebrafish through both forward genetic screens and TALEN-based genome editing approaches. These mutations result in early truncations of the protein; a few alleles at around 50 amino acids and one at 101 amino acids (Hartsock et al 2014; Deml et al, 2015). For our study we decided to use the CRISPR/Cas9 genome editing approach to generate a new zebrafish *mab21l2* allele. The novel line that we developed carries a 4-base pair deletion in the single exon of the *mab21l2* gene (*mab21l2*^{u517}). This deletion introduced a frame-shift mutation Lys43Argfs*13 (c.128_131delAGGA) that is predicted to truncate the protein by 317 amino acids with loss of the entire Mab-21 domain (Fig. 1A; Supplementary Fig. 1). We gauged the *mab21l2* mRNA levels in mutant embryos and ruled out a non-sense mediated decay process (Supplementary Fig. 1). The kind of truncation in the Mab21l2 protein together with the fact that the gene is encoded by a single exon suggested that the mutation was likely to result in a loss of function.

Homozygous *mab21l2*^{u517} mutants showed fully penetrant recessive microphthalmia and small or absent lens at 75 hpf, similar to other *mab21l2* alleles (Fig. 1B, C; Deml et al., 2015; Gath & Gross, 2019; Hartsock et al., 2014). The microphthalmic phenotype is characterised by eyes flattened along the dorsal ventral axis (Fig. 1C). Consistent with published data, mutants displayed also variable coloboma (not shown) (Deml *et al.*, 2015; Gath and Gross, 2019).

In zebrafish, mutants that display abnormalities at the CMZ often exhibit arrest in eye growth and microphthalmia (Cerveny *et al.*, 2010; Marcus *et al.*, 1999; Raymond *et al.*, 2006; Valdivia *et al.*, 2016; Wehman *et al.*, 2005). Thus, we first investigated if there were abnormalities in *mab21l2*^{u517} mutant eyes at 75hpf when all retinal growth derives from the CMZ. We analysed the expression of *cyclin D1* (*ccnd1*) as a broad marker for proliferative progenitors in the CMZ (Cerveny *et al.*, 2010). *Ccnd1* encodes a G1 cyclin and facilitates cell cycle progress and proliferation (Green *et al.*, 2003); Cerveny et al, 2010). In wildtype conditions, *ccnd1* is expression is restricted to a region surrounding the lens marking proliferative RPCs in the CMZ (Cerveny *et al.*, 2010; Valdivia *et al.*, 2016). In contrast, we found that *ccnd1* expression is expanded in the mutant and spans almost the whole eye, suggesting that a higher number of cells may be allocated in the CMZ (Fig. 1D, E). Consistently, quantification of cell nuclei in the CMZ revealed a significantly higher number of cells per area of the section in mutants compared to siblings (Fig. 1 F-H).

These results show that the small eye phenotype in *mab21l2*^{u517} mutant is not due to a smaller CMZ. Although *mab21l2* is expressed in the zebrafish CMZ, the transcripts are also found in the eye field, optic vesicles, and cups (Deml *et al.*, 2015; Kudoh and Dawid, 2001). Moreover, *mab21l2* has been shown to be one of the early effectors of *rx3*, a key transcriptional regulator of eye formation in zebrafish (Kennedy *et al.*, 2004; Yin *et al.*, 2014). Therefore, the expanded CMZ could be a consequence of aberrant early eye morphogenesis.

Optic cup morphogenesis requires *mab21l2* activity

To gain insight into the morphogenetic mechanisms shaping the *mab21l2*^{u517} mutant eye, we immunodetected green fluorescent protein (GFP) in wildtype and *mab21l2*^{u517} embryos carrying the *tg(vsx2:GFP)*^{nns1} transgene(Kimura *et al.*, 2006; Vitorino *et al.*, 2009). *vsx2* encodes a homeodomain transcription factor that is initially

expressed in multipotent zebrafish retinal progenitor cells and becomes restricted later to a subset of bipolar cells and Müller glia, as well as to the CMZ (Vitorino *et al.*, 2009).

We first imaged *tg(vsx2:GFP)*^{nns1} transgenic embryos at 18hpf, when optic cup morphogenesis has recently started (Kwan *et al.*, 2012; Li *et al.*, 2000; Nicolás-Pérez *et al.*, 2016). The expression of the transgene is clearly seen in the folding wildtype retina (Fig. 2A). GFP expression is strongly reduced in *mab21l2*^{u517} mutant eyes at the same stage (Fig. 2C), potentially as a consequence of *mab21l2* controlling the expression of *vsx2* during eye development (Sghari and Gunhaga, 2018; Yamada *et al.*, 2004). At this stage, there was no difference in the eye size between wildtype and mutants (Fig. 2C and data not shown).

Given the importance of epithelial polarization in driving tissue morphogenesis, we examined the organization of the basal lamina in *mab21l2*^{u517} mutant eyes. Laminin-1 deposition at the basal feet of the retinal cells is essential for the folding of the retinal neuroepithelium (Nicolás-Pérez *et al.*, 2016). While Laminin-1 accumulated at the point of optic cup folding in sibling eyes (Figure 2B; arrowheads), its deposition was strongly reduced in mutants (Fig. 2C, D).

At 24hpf, the expression of *tg(vsx2:GFP)*^{nns1} was relatively uniform throughout the optic cup in siblings' eyes (Fig. 3A). At this stage, the small eye phenotype was evident in mutants (Fig. 3B, M). The invagination of the optic vesicle started in the *mab21l2*^{u517}mutants but its rotation was delayed and nasal and temporal domains of the cups were not yet visible (Fig.3B; Picker et al., 2009; Schmitt & Dowling, 1994) GFP expression was still reduced in mutant eyes compared to siblings even though a trail of stronger GFP-positive cells in the ventro-nasal region of the mutant eyes was present (Fig.3B; arrowhead). These defects are consistent with an arrest of the so-called epithelial flow which is required for moving cells around the rims of the developing cup (Heermann *et al.*, 2015; Picker *et al.*, 2009).

By using DAPI nuclear staining we observed signs that the gastrulation-like cell movements of the eye from the lens-averted into the lens-facing epithelium of the developing optic cup of the eye is disrupted in *mab21l2*^{u517} (Fig. 3I,J) (Heermann *et al.*, 2015).

At 33hpf, the expression of *vsx2* reporter remained reduced in *mab21l2*^{u517} eyes compared to siblings (Fig. 3C, D). Distinctive non-fluorescent gaps within the GFP-expressing domain in transgenic embryos were observed in mutant retinas (Fig.3D), with a transient groove/sulcus in the dorsal eye where the dorsal vessel was forming (Hocking et al., 2018). GFP expression was stronger and showed less gaps in the nasal than temporal retina (Fig. 3D). Indeed, in the mutants, the nasal domain appeared better organized than the temporal portion of the retina while the control situation was more symmetric, suggesting that less cells were populating the temporal retina in *mab21l2*^{u517} mutants compared to wildtype. A 3D rendering of siblings and mutant eyes highlights these differences and suggest that nasal/temporal patterning mechanisms may be implicated in the *mab21l2*^{u517}phenotype (Fig. 3K, L).

Later during development, *tg(vsx2:GFP)*^{nns1} expression became similar between mutant and control eyes. Sibling eyes were mostly symmetrical in shape at 48hpf whereas mutants showed microphthalmia with a flattening of the eye along the dorsal-ventral axis. The asymmetry along the nasal-temporal axis persisted, such that the nasal retina protruded more than then temporal portion (Fig. 3E, F). The groove in the dorsal retina observed at 33hpf was more pronounced in *mab21l2*^{u517} eyes at 48hpf (Fig.3F, arrowhead). By 75hpf the ectopic groove was not easily observed in *mab21l2*^{u517}. The lens was severely reduced or absent in mutants at 75hpf (Fig.3G, H;

asterisk), which is consistent with previous studies (Deml *et al.*, 2015; Gath and Gross, 2019; Hartsock *et al.*, 2014).

To explore how the small eye phenotype evolves during *mab21l2*^{u517}eye morphogenesis, we measured eye size in *mab21l2*^{u517} mutants at 24, 30 and 52 hpf. In mutants, eye volumes from retinal profiles were consistently reduced to 60% of the volume of their wild-type siblings at all the stages analysed (Fig. 3M).

Together, these results suggest that loss of *mab21l2* function results in defective morphogenesis between 18 and 75hpf and compromised eye growth from before 24hpf.

Changes in expression of *cyclin D1* correlate with a delay during eye morphogenesis in *mab21l2*^{u517} *mutants*

The mouse *Vsx2 (Chx10)* gene is required for normal expression of *Cyclin D1* (*Ccnd1)* in developing eyes. *Chx10*-null retinae display reduced cell numbers due to a change in the balance of *Ccnd1* and *P27Kip1* expression (Green *et al.*, 2003). Having described that the reporter of *vsx2* expression is downregulated at early stages of optic cup morphogenesis in *mab21l2*^{u517} eyes, we asked whether this regulatory hierarchy may have consequences for expression of *ccnd1* in the transition from proliferation to differentiation in zebrafish eyes.

We performed a time course of *ccnd1* expression in *mab21l2*^{u517} embryos using *in situ* hybridization, starting at 28hpf when neurogenesis initiates in the zebrafish retina (Hu and Easter, 1999; Masai *et al.*, 2000). The broad and strong *ccnd1* expression observed in wildtype eyes between 28-36 hpf, became progressively restricted to the CMZ from 48hpf (Fig 4 A, C, E). In contrast, *mab21l2*^{u517} eyes showed reduced levels of *ccnd1* staining at 28hpf and 36hpf. *ccnd1* staining was stronger and broader than siblings at later stages of development. At 48 hpf, *ccnd1* expression in the mutants was comparable to the staining observed in siblings at 28hpf and 36hpf (Fig 4A, C, F) and it was only by 75hpf that *ccnd1* expression becomes more restricted to the CMZ (Fig 4G-J). This suggests that in *mab21l2*^{u517}mutants the spatial changes in *ccnd1* expression are shifted to later stages of development.

Previous studies in knockout mice for *Mab21l2* have shown that the microphthalmia phenotype is due to a decrease in cell proliferation in the developing optic vesicles (Yamada *et al.*, 2004). Conversely, *mab21l2* morpholino-injected zebrafish embryos showed no overt difference in cell proliferation (Kennedy *et al.*, 2004). In other zebrafish *mab21l2* alleles (*mab21l2*$^{Q48Sfs\_5}$ *and mab21l2*$^{R51\_F52del}$), qualitative analyses of cell proliferation revealed allele specific differences of PCNA (*proliferating cell nuclear antigen*) staining that seemed to be reduced in *mab21l2*$^{Q48Sfs\_5}$ and mis-patterned in *mab21l2*$^{R51\_F52del}$ (Deml *et al.*, 2015). To quantify proliferation in the *mab21l2*^{u517} allele, we performed phospho-histone 3 (PH3) immunostaining to detect cells undergoing mitosis. Although total eye mitotic figures were reduced in mutants compared to siblings at each stage analysed (data not shown), when standardized by the area of the eye we found decreased proliferation only at 30hpf (Fig. 4K). This change precedes the differential malformations along the nasal temporal axis of the eye at 33hpf (Fig 3D), suggesting that a drop in cell proliferation at a defined time point could contribute to such defects.

Together, these data show that the small eye phenotype in *mab21l2*^{u517} is accompanied by a shift in the timing of expression of *ccnd1*, suggesting a delay during eye development. Quantification of mitotic figures standardized by the size of the organ

did not reveal gross differences in *mab21l2*^{u517} eyes, except at a timepoint that precedes morphogenetic differences along the nasal temporal axis.

Progression of differentiation wave is slowed in *mab21l2*^{u517} retinae.

Further maturation of the optic cup involves the transition from proliferation to differentiation of retinal progenitors to give rise to all the neuronal and glial cell types that compose the retina (Boije *et al.*, 2014; Livesey and Cepko, 2001). In the zebrafish eyes, neurogenesis takes place in waves in an almost invariant sequence where nascent retinal ganglion cells (RGCs) are the first neurons to be born and they can be visualised by tracking the expression of the *basic helix-loop-helix* transcription factor encoding gene *atoh7* (Masai *et al.*, 2000; Neumann and Nuesslein-Volhard, 2000; Poggi *et al.*, 2005; Shen and Raymond, 2004). Given that neurogenesis may be linked to morphogenesis in the zebrafish eyes (Masai *et al.*, 2000; Neumann and Nuesslein-Volhard, 2000; Shen and Raymond, 2004; Zolessi *et al.*, 2006), we next asked whether the nasal-temporal malformations observed in *mab21l2*^{u517} eyes are correlated with defective propagation of the neurogenic wave along that axis.

In control eyes at 28 hpf, *atoh7* was expressed in a defined patch of nasal-ventral retinal multipotent progenitors and subsequently spreaded clockwise in a wave across the retina to produce neurons (Masai *et al.*, 2000) (Fig. 5A). In *mab21l2*^{u517} embryos, *atoh7* expression was induced at a similar timepoint than siblings but subsequent progression of the expression wave was delayed (Fig. 5B). Indeed, 36hpf-mutant retinas expressed *atoh7* exclusively in the nasal retina, similar to the 28hpf pattern in siblings (Fig. 5B, D). At 48 hpf we observed a burst of *atoh7* expression in mutants, similar to siblings at 36hpf (Fig. 5C, F). In register with *ccnd1* expression, this propagation of the neurogenesis coincided with the morphogenesis of the temporal retina in mutants at 48hpf. *atoh7* expression appeared to be slightly expanded in *mab21l2*^{u517} mutants eye compared to sibling eyes at 72hpf (Fig. 5G, H); but the lack of lens and the small eye phenotype in mutants made it difficult to confirm subtle differences.

To look at later neurogenic stages, we used a stable transgenic line *tg(atoh7:GAP-mRFP)*^{cu2} to report *atoh7* expression in transverse sections (Zolessi *et al.*, 2006). In mutants at 53 hpf, differentiating RGCs retained their epithelial features and displayed apical domains that are not retracted yet, a feature characteristic of early retinal progenitors (Poggi *et al.*, 2005; Zolessi *et al.*, 2006) (Fig. 5I,J; arrows). Additionally, nuclear staining showed a lack of lamination in the mutant retina at the same stage (Fig. 5I, J). Regardless of the delay in *atoh7* expression, we found that neurogenesis took place in mutant eyes and we could see the RGC and inner plexiform layers at 75 hpf, consistent with previous reports (Gath and Gross, 2019) (Supplementary Fig. 2). Together, these experiments indicate that neurogenesis is delayed in the *mab21l2*^{u517} mutants.

The transition from proliferation to differentiation can be studied in the embryonic retina but also in the CMZ. To provide further evidence that differentiation is delayed in the *mab21l2*^{u517} mutant retina, we performed BrdU incorporation at 54 hpf when the CMZ is becoming active (Stenkamp, 2007), and fixed the embryos at 100hpf. In contrast to siblings in which the development in the central retina is complete and proliferation is restricted to the peripheral CMZ, in *mab21l2*^{u517}mutants BrdU positive cells were distributed all over the retina suggesting that cells maintained proliferative features until later developmental stages (Figure 5K,L and 5K',L'). Consistent with previous data, mutant progenitors eventually differentiated into neurons (Gath & Gross, 2019 ; Supplementary Fig. 2). Overall, our results suggest that *mab21l2* loss of function leads to a developmental delay during retinal neurogenesis.

Discussion

Previous studies in vertebrate models have provided evidence of severe eye defects upon abrogation of *Mab21l2* gene function. The phenotypes include small or absent eyes, differentiation defects, and lens and cornea malformations (Deml *et al.*, 2015; Gath and Gross, 2019; Rainger *et al.*, 2014; Sghari and Gunhaga, 2018; Yamada *et al.*, 2004). Our work adds to such studies, revealing that *mab21l2* absence delays morphogenesis of the optic cup in zebrafish. This likely contributes to disrupted retinal neurogenesis and delayed establishment of the CMZ. Defective morphogenesis, characterised by malformations of the optic cup along the nasal-temporal axis, correlates with delayed progression of neurogenesis in the temporal half of the eye. Our data suggest that developmental delay might underlie the microphthalmic phenotype in vertebrates carrying *mab21l2* mutations, and that *mab21l2* directly or indirectly regulate retinal neurogenesis linking morphogenesis and differentiation.

-Mab21l2 influences the timing of eye development

A key regulator of eye formation in zebrafish, *rx3*, controls the expression of a defined set of genes that include *mab21l2* (Kennedy *et al.*, 2004; Yin *et al.*, 2014). The set of regulated genes also includes *vsx2*, which encodes a conserved homeobox transcription factor (Vitorino *et al.*, 2009). It has been shown that expression of *Chx10/Vsx2* is significantly reduced in *Mab21l2*-null mice embryos (Yamada *et al.*, 2004). In our study we used a *bonafide vsx2* transgenic reporter (Vitorino *et al.*, 2009) and found that *vsx2* expression is not lost but markedly delayed in *mab21l2*^{u517} eyes suggesting an indirect or perhaps partial role for *mab21l2* in regulation of *vsx2*.

Knockdown of *vsx2* in fish induces microphthalmia, impaired optic cup formation and coloboma (Gago-Rodrigues *et al.*, 2015; Vitorino *et al.*, 2009). *vsx2* directly regulates the transcriptional levels of the *ojoplano* (*opo*) gene, which encodes a transmembrane protein that transmits mechanical forces for optic cup morphogenesis (Martinez-Morales *et al.*, 2009). When mutated, *opo* leads to severe defects in optic cup formation (Martinez-Morales *et al.*, 2009). It is possible that altered *vsx2* expression in *mab21l2*^{u517} embryos contributes to the early optic cup defects mediated at least in part by zebrafish *opo*.

Cell-tracking experiments of zebrafish eye morphogenesis have shown extensive cell movements during optic vesicle evagination and optic cup formation (Heermann *et al.*, 2015; Ivanovitch *et al.*, 2013; Kwan *et al.*, 2012; Picker *et al.*, 2009). We provide evidence that loss of *mab21l2* function results in eye malformations in zebrafish embryos as early as 18 hpf characterized by a profound delay in eye development. At 24hpf we found a disruption in the organization of the cells that flow around the margin of the forming optic cup, which becomes more severe at the temporal retina by 33 hpf.

It has been proposed that presumptive stem cells of the CMZ originate from the region of the optic vesicle that is closer to the body midline, and then migrate around the rims of developing eyes to their appropriate destination at the margin of the retina (Heermann *et al.*, 2015; Kwan *et al.*, 2012). Disruption of whole epithelium displacement has, therefore, consequences for allocating cells to the CMZ (Heermann *et al.*, 2015). Our data indicates that morphogenetic defects observed in *mab21l2*^{u517} eyes are consistent with an abnormal CMZ formation. Together with our findings that *ccnd1* expression follows a pattern that spans most of the early eye to become restricted to the CMZ, we propose that the delay in *mab21l2*^{u517} morphogenesis may result in cells arriving later to the CMZ while they are still expressing high levels of

ccnd1. It is tempting to speculate that *mab21l2* may facilitate the epithelial flow during optic cup morphogenesis (Heermann *et al.*, 2015).

-Mab21l2 links morphogenesis and differentiation

Growth of embryonic mouse eyes requires *Chx10/Vsx2* to regulate proliferation of retinal progenitor cells, as revealed in *Ocular Retardation* mutants that exhibit microphthalmia (Burmeister *et al.*, 1996; Ferda Percin *et al.*, 2000). Importantly, *Chx10/Vsx2* is also required for normal *Ccnd1* expression in mouse developing eyes (Green *et al.*, 2003), which is consistent with our findings of a delay in the expression of *ccnd1* in *mab21l2^{u517}*. Although the small eye phenotype at 24hpf in *mab21l2^{u517}* is consistent also with the delay in GFP expression observed in *tg(vsx2:GFP)^{nns1}*, we found no significant differences in the number of mitotic figures per area during eye development, except in a specific timepoint at 30hpf. As mutant eyes are smaller as early as 24hpf, this suggests that additional mechanisms such as increased cell death (Deml *et al.*, 2015; Kennedy *et al.*, 2004) or cell size changes could play a role in controlling eye size in *mab21l2^{u517}*.

A striking phenotype of *mab21l2^{u517}* eyes is the asymmetric retina along the nasal-temporal axis at 33hpf, characterized by an abnormal temporal portion of the eye. Interestingly, this malformation correlates with a failure on nasal-temporal propagation of the *atoh7*-dependent neurogenic wave (Masai *et al.*, 2000) and is preceded by a drop in proliferation in developing eyes at 30hpf. *atoh7* expression propagates to the temporal retina only by 48hpf,when the cup is formed in mutants. These findings support the idea that morphogenesis must be tightly coordinated with differentiation.

We also provided evidence that the transition from proliferation to differentiation takes place later than normal in *mab21l2^{u517}* mutant eyes. We gave BrdU pulses at 54 hpf when most of the cells are post mitotic in the retina and neurogenesis comes almost exclusively from the CMZ in wildtypes (Stenkamp, 2007). Neurons and glia are thus locally produced at the margin of the eye and added in the growing retina to be included in all the layers (Stenkamp, 2007). If there was a delay in development in *mab21l2^{u517}* mutants, we should expect to observe more BrdU-labelled cells in the central retina. Indeed, we found that these BrdU positive cells are distributed mainly in the inner nuclear layer (INL) of the *mab21l2^{u517}* retina (Figure 5M', N'). Our interpretation is that the BrdU pulse was given at a time point in which late retinal cell types that populate the INL were still being produced after a late differentiation of the RGCs. Therefore, retinal precursors in *mab21l2^{u517}*undergo proliferation when precursors in wildtype eyes are already producing neurons.

Overall, we propose that *mab21l2* links morphogenesis and differentiation. *mab21l2* contributes to setting the timing of RPCs differentiation, which is likely linked to the aberrant morphogenesis of the optic cup. These data suggest that cells shift their proliferative dynamics to later stages development. Eye formation is delayed in mutants resulting in a CMZ made of “younger” cells.

-How might the absence of mab21l2 result in small eyes and delayed neurogenesis?

During optic cup morphogenesis, the process known as epithelial flow is facilitated by modulation of BMP signalling in zebrafish (Heermann *et al.*, 2015). The *mab21l2^{u517}* phenotype is similar to a BMP gain of function, which impairs the movement of cells that shape the optic cup (Heermann *et al.*, 2015). Functionally, Mab21l2 antagonizes BMP signalling through physical interaction with the

transcriptional effector Smad1 in *Xenopus* gastrulae (Baldessari *et al.*, 2004). This is reminiscent of the role of *mab-21* in *C. elegans*, where it interacts genetically with *cet-1*, whose vertebrate paralogs are the proteins *Bmp2*, *Bmp4*, and *Bmp7* (Chow *et al.*, 1995; Choy *et al.*, 2007). Similar to *mab21l2*, BMP signalling is also important for eye development: mutations in factors such as *BMP4*, *BMP7*, and *GDF6* lead to an overlapping spectrum of human eye phenotypes (Reis and Semina, 2015). *gdf6a* deficiency results also in reduced *smad1* expression and small eyes in fish (Pant et al, 2013). An attractive possibility is that *mab21l2* may mediate the epithelial flow by interacting with BMP members during vertebrate eye formation in an evolutionary conserved interaction.

The neurogenic delay in *mab21l2*^{u517} mutant eyes may be a consequence of either aberrant morphogenesis or due to a direct impact on neurogenesis. In chicken, *mab21l2* has a stage dependent role on eye formation and loss of function of the gene impairs in neuronal differentiation (Sghari and Gunhaga, 2018). However, this seems to be different in zebrafish as we and others have shown that neurons are indeed produced in mutants (this work; Gath & Gross, 2019) though we do find defects related to delays in neurogenesis. In *C. elegans*, *mab-21* also interacts genetically and physically with *sin-3*/SIN-3, a co-repressor that forms complexes with histone deacetylases (HDAC) (Choy *et al.*, 2007; Kuzmichev et al., 2002), . In zebrafish, *hdac1* regulates retinal neurogenesis in zebrafish by suppressing Wnt and Notch signalling pathways (Yamaguchi *et al.*, 2005); a *hdac1* mutation result in defects characterized by a failure in propagation of neurogenesis and cells are kept in a proliferative state for longer (Yamaguchi *et al.*, 2005). Our data are consistent with the idea that an interaction between *mab21l2/HDAC* may be conserved in vertebrate eye development.

Our findings add to a growing understanding of the role of *mab21l2* in vertebrate eye formation. They provide leads for future work to unveil molecular links between morphogenesis and neurogenesis in developing eyes.

Acknowledgements

This work was funded by grants from FONDECYT (grant 11160951 to L.E.V), CONICYT International network grants (REDI170300 and REDES170010 to L.E.V), the Medical Research Council [MR/L003775/1 to Stephen Wilson and G.G], Universidad Mayor FDP grant (PEP I-2019074 to L.E.V.) and Universidad Mayor Start up grant (I-2018005 to L.E.V). We are grateful to Stephen Wilson and Joaquin Letelier for helpful comments on the manuscript.

References

BALDESSARI D, BADALONI A, LONGHI R, ZAPPAVIGNA V, CONSALEZ GG (2004). MAB21L2, a vertebrate member of the Male-abnormal 21 family, modulates BMP signaling and interacts with SMAD1. *BMC Cell Biol* 5: 1–14.

BAZIN-LOPEZ N, VALDIVIA LE, WILSON SW, GESTRI G (2015). Watching eyes take shape. *Curr Opin Genet Dev* 32: 73–79. Available at: http://dx.doi.org/10.1016/j.gde.2015.02.004.

BOIJE H, MACDONALD RB, HARRIS WA (2014). Reconciling competence and transcriptional hierarchies with stochasticity in retinal lineages. *Curr Opin Neurobiol* 27: 68–74. Available at: http://dx.doi.org/10.1016/j.conb.2014.02.014.

BURMEISTER M, NOVAK J, LIANG MY, BASU S, PLODER L, HAWES NL, VIDGEN D, HOOVER F, GOLDMAN D, KALNINS VI, RODERICK TH, TAYLOR BA, HANKIN MH, MCINNES RR (1996). Ocular retardation mouse caused by Chx10 homeobox null allele: Impaired retinal progenitor proliferation and bipolar cell differentiation. *Nat Genet* 12: 376–384.

CAVODEASSI F, HOUART C (2012). Brain regionalization: Of signaling centers and boundaries. *Dev Neurobiol* 72: 218–233.

CENTANIN L, HOECKENDORF B, WITTBRODT J (2011). Fate restriction and multipotency in retinal stem cells. *Cell Stem Cell* 9: 553–562.

CERVENY KL, CAVODEASSI F, TURNER KJ, DE JONG-CURTAIN TA, HEATH JK, WILSON SW (2010). The zebrafish flotte lotte mutant reveals that the local retinal environment promotes the differentiation of proliferating precursors emerging from their stem cell niche. *Development* 137: 2107–2115.

CHOW KL, EMMONS SW (1994). HOM-C/Hox genes and four interacting loci determine the morphogenetic properties of single cells in the nematode male tail. *Development* 120: 2579–2592.

CHOW KL, HALL DH, EMMONS SW (1995). The mab-21 gene of Caenorhabditis elegans encodes a novel protein required for choice of alternate cell fates. *Development* 121: 3615–3626.

CHOW RL, LANG RA (2001). Early eye development in vertebrates. *Annu Rev Cell Dev Biol* 17: 255–296.

CHOY SW, WONG YM, HO SH, CHOW KL (2007). C. elegans SIN-3 and its associated HDAC corepressor complex act as mediators of male sensory ray development. *Biochem Biophys Res Commun* 358: 802–807.

DAHLEM TJ, HOSHIJIMA K, JURYNEC MJ, GUNTHER D, STARKER CG, LOCKE AS, WEIS AM, VOYTAS DF,GRUNWALD DJ (2012) Simple Methods for Generating and Detecting Locus-Specific Mutations Induced with TALENs in the Zebrafish Genome. *PLoS Genetics*. 8(8):e1002861.

DEML B, KARIMINEJAD A, BORUJERDI RHR, MUHEISEN S, REIS LM, SEMINA E V. (2015). Mutations in MAB21L2 Result in Ocular Coloboma, Microcornea and Cataracts. *PLoS Genet* 11: 1–26.

FANTES J, RAGGE NK, LYNCH SA, MCGILL NI, COLLIN JRO, HOWARD-PEEBLES PN, HAYWARD C, VIVIAN AJ, WILLIAMSON K, VAN HEYNINGEN V, FITZPATRICK DR (2003). Mutations in SOX2 cause anophthalmia. *Nat Genet* 33: 461–463.

FERDA PERCIN E, PLODER LA, YU JJ, ARICI K, JONATHAN HORSFORD D, RUTHERFORD A, BAPAT B, COX DW, DUNCAN AMV, KALNINS VI, KOCAK-ALTINTAS A, SOWDEN JC, TRABOULSI E, SARFARAZI M, MCINNES RR (2000). Human microphthalmia associated with mutations in the retinal homeobox gene CHX10. *Nat Genet* 25: 397–401.

FUHRMANN S (2010). *Eye morphogenesis and patterning of the optic vesicle*. Elsevier Inc. Available at: http://dx.doi.org/10.1016/B978-0-12-385044-7.00003-5.

GAGO-RODRIGUES I, FERNÁNDEZ-MIÑÁN A, LETELIER J, NARANJO S, TENA JJ, GÓMEZ-SKARMETA JL, MARTINEZ-MORALES JR (2015). Analysis of opo cis-regulatory landscape uncovers Vsx2 requirement in early eye morphogenesis. *Nat Commun* 6.

GATH N, GROSS JM (2019). Zebrafish mab21l2 mutants possess severe defects in optic cup morphogenesis, lens and cornea development. *Dev Dyn* 248: 514–529.

GERTH-KAHLERT C, WILLIAMSON K, ANSARI M, RAINGER JK, HINGST V, ZIMMERMANN T, TECH S, GUTHOFF RF, HEYNINGEN V van, FITZPATRICK DR (2013). Clinical and mutation analysis of 51 probands with anophthalmia and/or severe microphthalmia from a single center. *Mol Genet Genomic Med* 1: 15–31.

GREEN ES, STUBBS JL, LEVINE EM (2003). Genetic rescue of cell number in a mouse model of microphthalmia: Interactions between Chx10 and G1-phase cell cycle regulators. *Development* 130: 539–552.
HARTSOCK A, LEE C, ARNOLD V, GROSS JM (2014). In vivo analysis of hyaloid vasculature morphogenesis in zebrafish: A role for the lens in maturation and maintenance of the hyaloid. *Dev Biol* 394: 327–339. Available at: http://dx.doi.org/10.1016/j.ydbio.2014.07.024.
HEERMANN S, SCHÜTZ L, LEMKE S, KRIEGLSTEIN K, WITTBRODT J (2015). Eye morphogenesis driven by epithelial flow into the optic cup facilitated by modulation of bone morphogenetic protein. *Elife* 4: 1–17.
HU M, EASTER J (1999). Retinal neurogenesis: The formation of the initial central patch of postmitotic cells. *Dev Biol* 207: 309–321.
HWANG WY, FU Y, REYON D, MAEDER ML, TSAI SQ, SANDER JD, PETERSON RT, YEH JR, JOUNG JK (2013) Efficient genome editing in zebrafish using a CRISPR-Cas system. *Nat. Biotechnol.. 31(3):227-229.*
IVANOVITCH K, CAVODEASSI F, WILSON SW (2013). Precocious Acquisition of Neuroepithelial Character in the Eye Field Underlies the Onset of Eye Morphogenesis. *Dev Cell* 27: 293–305. Available at: http://dx.doi.org/10.1016/j.devcel.2013.09.023.
JAO LE, WENTE SR, CHEN W. (2013) Efficient multiplex biallelic zebrafish genome editing using a CRISPR nuclease system. *Proceedings of the National Academy of Sciences of the United States of America*. 110(34):13904-13909.
KENNEDY BN, STEARNS GW, SMYTH VA, RAMAMURTHY V, VAN EEDEN F, ANKOUDINOVA I, RAIBLE D, HURLEY JB, BROCKERHOFF SE (2004). Zebrafish rx3 and mab21l2 are required during eye morphogenesis. *Dev Biol* 270: 336–349.
KIMMEL CB, BALLARD WW, KIMMEL SR, ULLMANN B, SCHILLING TF (1995). Stages of Embryonic Development of the Zebrafish. *Dev Dyn* 10.
KIMURA Y, OKAMURA Y, HIGASHIJIMA SI (2006). alx, a zebrafish homolog of Chx10, marks ipsilateral descending excitatory interneurons that participate in the regulation of spinal locomotor circuits. *J Neurosci* 26: 5684–5697.
KUDOH T, DAWID IB (2001). Zebrafish mab21l2 is specifically expressed in the presumptive eye and tectum from early somitogenesis onwards. *Mech Dev* 109: 95–98.
KUZMICHEV A, ZHANG Y, ERDJUMENT-BROMAGE H, TEMPST P, REINBERG D. (2002) Role of the Sin3-histone deacetylase complex in growth regulation by the candidate tumor suppressor p33(ING1). *Mol. Cell. Biol.* 22, 835–848
KWAN KM, OTSUNA H, KIDOKORO H, CARNEY KR, SAIJOH Y, CHIEN C Bin (2012). A complex choreography of cell movements shapes the vertebrate eye. *Development* 139: 359–372.
LI Z, JOSEPH NM, EASTER SS (2000). The morphogenesis of the zebrafish eye, including a fate map of the optic vesicle. *Dev Dyn* 218: 175–188.
LIVESEY FJ, CEPKO CL (2001). VERTEBRATE NEURAL CELL-FATE DETERMINATION : LESSONS FROM THE RETINA. *Nat Rev Neurosci* 2: 109–118.
MARCUS RC, DELANEY CL, EASTER SS (1999). Neurogenesis in the visual system of embryonic and adult zebrafish (Danio rerio). : 417–424.
MARIANI M, CORRADI A, BALDESSARI D, MALGARETTI N, POZZOLI O, FESCE R, MARTINEZ S, BONCINELLI E, CONSALEZ GG (1998). Mab21, the mouse homolog of a C. elegans cell-fate specification gene, participates in cerebellar, midbrain and eye development. *Mech Dev* 79: 131–135.
MARTINEZ-MORALES JR, CAVODEASSI F, BOVOLENTA P (2017). Coordinated morphogenetic mechanisms shape the vertebrate eye. *Front Neurosci* 11: 1–8.
MARTINEZ-MORALES JR, REMBOLD M, GREGER K, SIMPSON JC, BROWN KE, QUIRING R, PEPPERKOK R, MARTIN-BERMUDO MD, HIMMELBAUER H,

WITTBRODT J (2009). Ojoplano-Mediated Basal Constriction Is Essential for Optic Cup Morphogenesis. *Development* 136: 2165–2175. Available at: http://dev.biologists.org/cgi/doi/10.1242/dev.033563.
MASAI I, STEMPLE DL, OKAMOTO H, WILSON SW (2000). Midline signals regulate retinal neurogenesis in zebrafish. *Neuron* 27: 251–263.
MEEKER ND, HUTCHINSON SA, HO L, TREDE NS (2007). Method for isolation of PCR-ready genomic DNA from zebrafish tissues. *Biotechniques* 43: 610–614.
NEUMANN CJ, NUESSLEIN-VOLHARD C (2000). Patterning of the zebrafish retina by a wave of sonic Hedgehog activity. *Science (80-)* 289: 2137–2139.
NICOLÁS-PÉREZ M, KUCHLING F, LETELIER J, POLVILLO R, WITTBRODT J, MARTÍNEZ-MORALES JR (2016). Analysis of cellular behavior and cytoskeletal dynamics reveal a constriction mechanism driving optic cup morphogenesis. *Elife* 5: 1–24.
PANT SD, MARCH LD, FAMULSKI JK, FRENCH CR, LEHMANN OJ, WASKIEWICZ AJ. (2013) Molecular mechanisms regulating ocular apoptosis in zebrafish gdf6a mutants. *Investigative ophthalmology & visual science*. 54(8):5871-5879.
PICKER A, CAVODEASSI F, MACHATE A, BERNAUER S, HANS S, ABE G, KAWAKAMI K, WILSON SW, BRAND M (2009). Dynamic coupling of pattern formation and morphogenesis in the developing vertebrate retina. *PLoS Biol* 7.
POGGI L, VITORINO M, MASAI I, HARRIS WA (2005). Influences on neural lineage and mode of division in the zebrafish retina in vivo. *J Cell Biol* 171: 991–999.
RAINGER J, PEHLIVAN D, JOHANSSON S, BENGANI H, SANCHEZ-PULIDO L, WILLIAMSON KA, TURE M, BARKER H, ROSENDAHL K, SPRANGER J, et al. (2014). Monoallelic and biallelic mutations in MAB21L2 cause a spectrum of major eye malformations. *Am J Hum Genet* 94: 915–923.
RAYMOND PA, BARTHEL LK, BERNARDOS RL, PERKOWSKI JJ (2006). Molecular characterization of retinal stem cells and their niches in adult zebrafish. *BMC Dev Biol* 6: 1–17.
REINHARDT R, CENTANIN L, TAVHELIDSE T, INOUE D, WITTBRODT B, CONCORDET J, MARTINEZ-MORALES JR, WITTBRODT J (2015). Sox2, Tlx, Gli3, and Her9 converge on Rx2 to define retinal stem cells in vivo . *EMBO J* 34: 1572–1588.
REIS LM, SEMINA E V. (2015). Conserved genetic pathways associated with microphthalmia, anophthalmia, and coloboma. *Birth Defects Res Part C - Embryo Today Rev* 105: 96–113.
SCHMITT EA, DOWLING JE (1994). Early-eye morphogenesis in the zebrafish, Brachydanio rerio. *J Comp Neurol* 344: 532–542.
SGHARI S, GUNHAGA L (2018). Temporal requirement of mab21l2 during eye development in chick reveals stage-dependent functions for retinogenesis. *Investig Ophthalmol Vis Sci* 59: 3869–3878.
SHEN YC, RAYMOND PA (2004). Zebrafish cone-rod (crx) homeobox gene promotes retinogenesis. *Dev Biol* 269: 237–251.
STENKAMP DL (2007). Neurogenesis in the Fish Retina. *Int Rev Cytol* 259: 173–224.
THISSE C, THISSE B (2008). High-resolution in situ hybridization to whole-mount zebrafish embryos. *Nat Protoc* 3: 59–69.
TSANG SW, GUO Y, CHAN LH, HUANG Y, CHOW KL (2018). Generation and characterization of pathogenic Mab21l2(R51C) mouse model. *Genesis* 56: 1–7.
VALDIVIA LE, LAMB DB, HORNER W, WIERZBICKI C, TAFESSU A, WILLIAMS AM, GESTRI G, KRASNOW AM, VLEESHOUWER-NEUMANN TS, GIVENS M, YOUNG RM, LAWRENCE LM, STICKNEY HL, HAWKINS TA, SCHWARZ QP, CAVODEASSI F, WILSON SW, CERVENY KL (2016). Antagonism between Gdf6a and retinoic acid pathways controls timing of retinal neurogenesis and growth of the eye in zebrafish. *Dev* 143: 1087–1098.
VITORINO M, JUSUF PR, MAURUS D, KIMURA Y, HIGASHIJIMA SI, HARRIS WA

(2009). Vsx2 in the zebrafish retina: Restricted lineages through derepression. *Neural Dev* 4.
WEHMAN AM, STAUB W, MEYERS JR, RAYMOND PA, BAIER H (2005). Genetic dissection of the zebrafish retinal stem-cell compartment. *Dev Biol* 281: 53–65.
WONG RLY, CHOW KL (2002). Depletion of Mab21l1 and Mab21l2 messages in mouse embryo arrests axial turning, and impairs notochord and neural tube differentiation. *Teratology* 65: 70–77.
WONG RLY, WONG HT, CHOW KL (1999). Genomic cloning and chromosomal localization of the mouse Mab21/2 locus. *Cytogenet Cell Genet* 86: 21–24.
WONG YM, CHOW KL (2002). Expression of zebrafish mab21 genes marks the differentiating eye, midbrain and neural tube. *Mech Dev* 113: 149–152.
YAMADA R, MIZUTANI-KOSEKI Y, KOSEKI H, TAKAHASHI N (2004). Requirement for Mab21l2 during development of murine retina and ventral body wall. *Dev Biol* 274: 295–307.
YAMAGUCHI M, TONOU-FUJIMORI N, KOMORI A, MAEDA R, NOJIMA Y, LI H, OKAMOTO H, MASAI I (2005). Histone deacetylase 1 regulates retinal neurogenesis in zebrafish by suppressing Wnt ad Notch signaling pathways. *Development* 132: 3027–3043.
YIN J, MORRISSEY ME, SHINE L, KENNEDY C, HIGGINS DG, KENNEDY BN (2014). Genes and signaling networks regulated during zebrafish optic vesicle morphogenesis. *BMC Genomics* 15.
ZOLESSI FR, POGGI L, WILKINSON CJ, CHIEN C Bin, HARRIS WA (2006). Polarization and orientation of retinal ganglion cells in vivo. *Neural Dev* 1: 2.

Figures

Figure 1

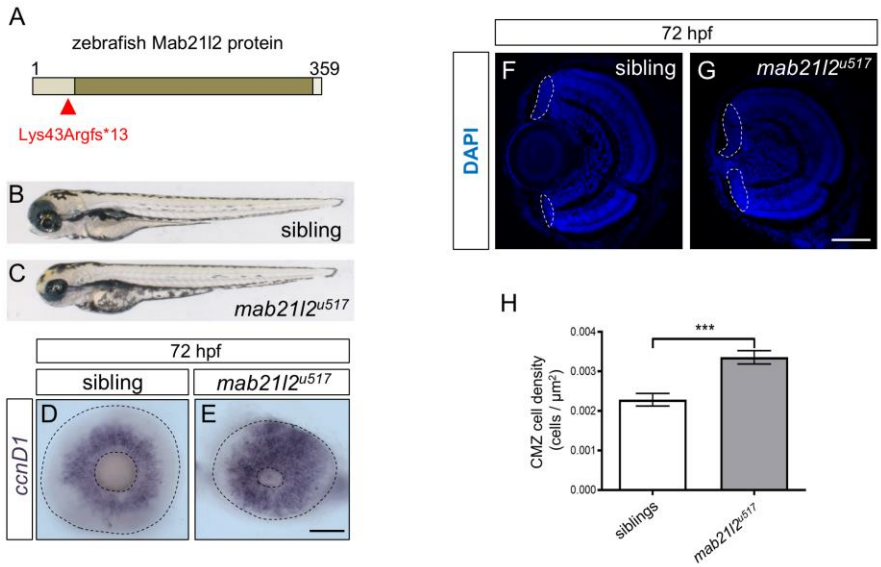

Figure 1. *mab21l2*^{u517} zebrafish mutants display microphthalmia associated with excessive cell numbers in the ciliary marginal zone (CMZ) of the eye. (A) Schematics of the zebrafish *Mab21l2* protein. The Mab-21 domain spans the amino acids 62–346 and is highlighted in dark brown colour; the position of the Lys43Argfs*13 mutation is indicated with a red arrowhead. (B, C) Lateral views of sibling (B), and *mab21l2*^{u517} mutants showing small eyes (C) at 72 hours post fertilization. (D, E) *ccnd1* is expressed more broadly in mutant eyes (E) compared with siblings (D). Dashed lines in (D) and (E) depict the eye tissue (outer line) and lens (inner line). (F, G) Transverse sections of eyes stained with DAPI highlighting a larger CMZ in *mab21l2*^{u517} (G) compared to siblings (F). (H) Nuclei contained inside the dashed white line limit (demarcating the boundary of the CMZ in F and G, based on nuclei morphology) were counted for siblings (n=9) and *mab21l2*^{u517} (n=12) embryos. The number of CMZ cells per area is increased in *mab21l2*^{u517}. Data was graphed with standard error bars (95% confidence limits; Student's t-test, ***P=0.0030). Scale bar = 50µm.

Figure 2

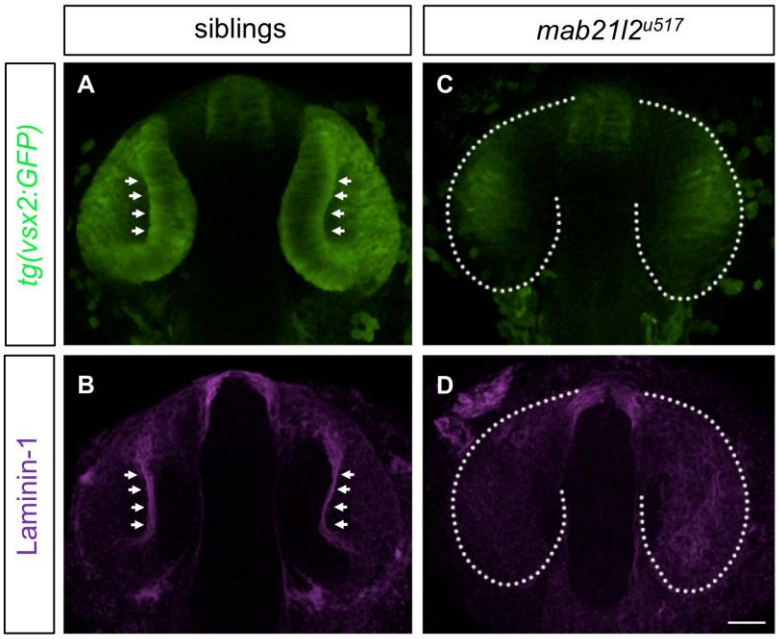

Figure 2. *mab21l2* loss of function affects initial optic cup formation. (A, C) Expression of the *tg(vsx2:GFP)*^{nns1} transgene, which labels retinal progenitor cells, in sibling (A) and *mab21l2*^{u517} (C). (B, D) Same embryos shown in (A) and (C) immunostained against Laminin-1. White arrows in (A) and (C) show the epithelializing cup and basally located Laminin-1, respectively. White dotted lines in (B) and (D) indicate the limits of the optic vesicles. All images are dorsal views at 18 hours post fertilization; anterior to the top; number of analysed specimens were n=7 and n=6 for siblings and mutants, respectively. Scale bar = 50µm.

Figure 3

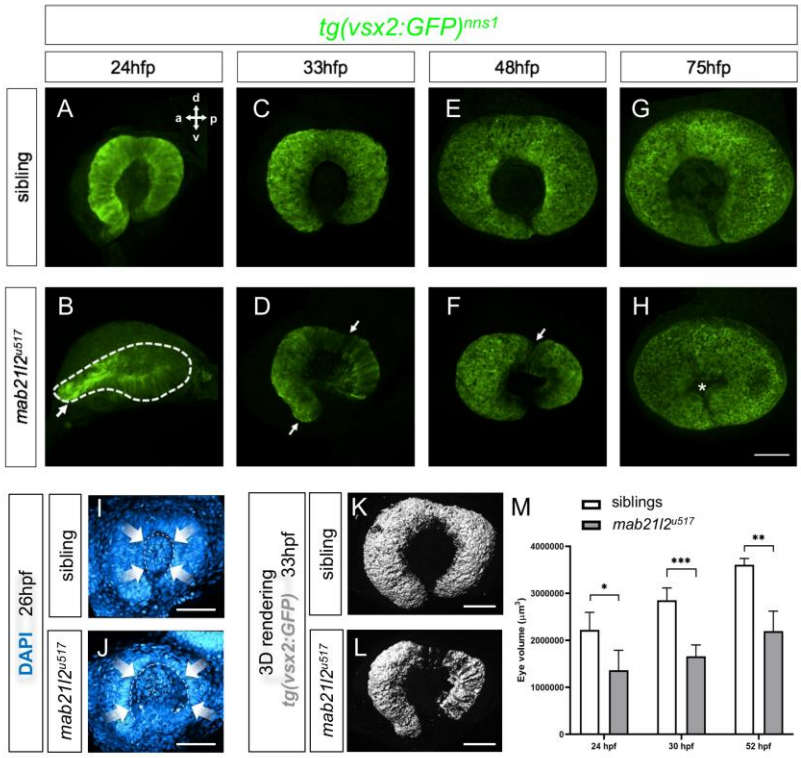

Figure 3. *mab21l2*^{u517} mutants have a complex eye morphogenesis phenotype. Confocal images of lateral views of whole-mount *mab21l2*^{u517}and sibling eyes at 24, 33, 48 and 75hpf, carrying the *tg(vsx2:GFP)*^{nns1} transgene. Sibling (A, C, E, G) and *mab21l2*^{u517} expression pattern (B, D, F, H). Embryos were immunostained for GFP (green). Retinal axes are shown as dorsal (d), ventral (v), anterior (a) and posterior (p). (I, J) lateral views of specimens with DAPI nuclear staining showing the organization of the developing eye at 24hpf. The mutants display an abnormal position of cells that flow around the rims of the eye (J) compared to siblings (I). Large white arrows show the direction of cell movements according to Heermann et al, 2015; small white arrows indicate pyknotic nuclei. (K, L) Three-dimensional renderings obtained from confocal data showing both wild-type (K) and *mab21l2*^{u517} mutant (L) *tg(vsx2:GFP)*^{nns1} transgenic eyes at 33hpf. The mutants display malformed temporal retina (right part of the eye) and superior coloboma. (M) Comparison of eye volume between siblings (number of analysed specimens: 24hpf = 5; 30hpf = 5; 52hpf = 5) and mutants (number of analysed specimens: 24hpf = 4; 30hpf = 11; 52hpf = 5) showing that the latter are smaller at all time points analysed (95% confidence limits; Mann-Whitney U test, p = *0,0159; **0,008; *** 0,0005). White arrowheads indicate the trail of GFP-positive cells at 24 and 33hpf (located bottom left in B and D), and the dorsal groove in mutant retinas at 33hpf and 48hpf (located upper). White asterisks (*) highlight the abnormally small lens in mutants at 75hpf. Scale bar = 50µm.

Figure 4

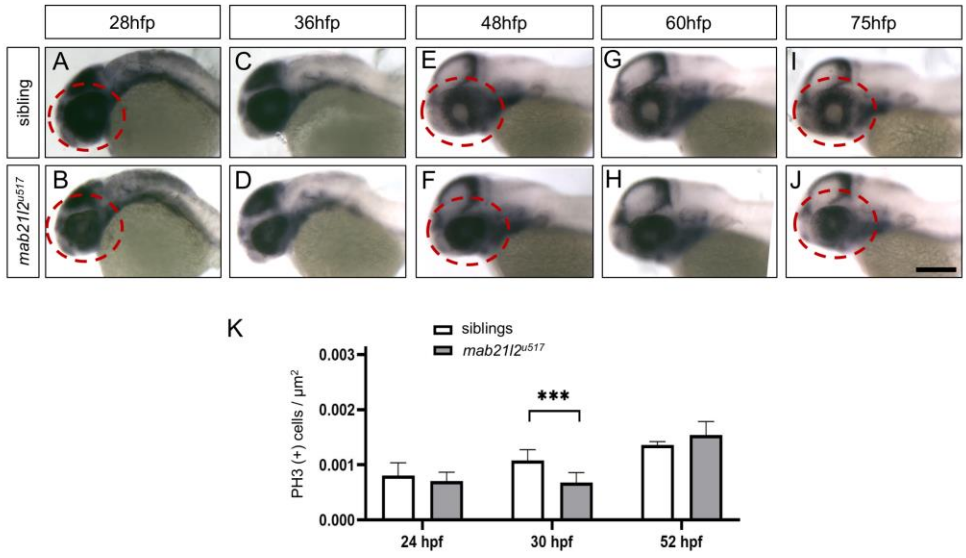

Figure 4. *mab21l2*^{u517} mutant eyes exhibit a temporal shift in the expression of the proliferative cell marker *cyclin D1* accompanied by a specific reduction in cell proliferation. (A-J) *ccnd1* expression in siblings and mutants. In the sibling retinae, *ccnd1* is highly expressed at 28 and 36 hpf and becomes restricted to the CMZ from 48hpf onwards. The *in situ* hybridization staining is fainter in mutants at 28 and 36 hpf but it becomes stronger at 48hpf and remains high in mutant eyes at 72hpf. Dashed lines in A-B, E-F, and I-J, highlight differences in *ccnd1* expression in the eye. (K) PH3 positive cells standardized by area show decreased proliferation only at 30hpf; other timepoint were not significantly different. This phenomenon precedes the nasal temporal malformations in mutants. (95% confidence limits; Mann-Whitney U test, p = *0,0159; **0,008; *** 0,0005). Number of analysed sibling specimens at 24hpf, 30hpf, and 52h, were 5 in each timepoint; Number of analysed mutant specimens at 24hpf, 30hpf, and 52h, were 4, 5 and 11, respectively). Scale bar = 200 µm

Figure 5

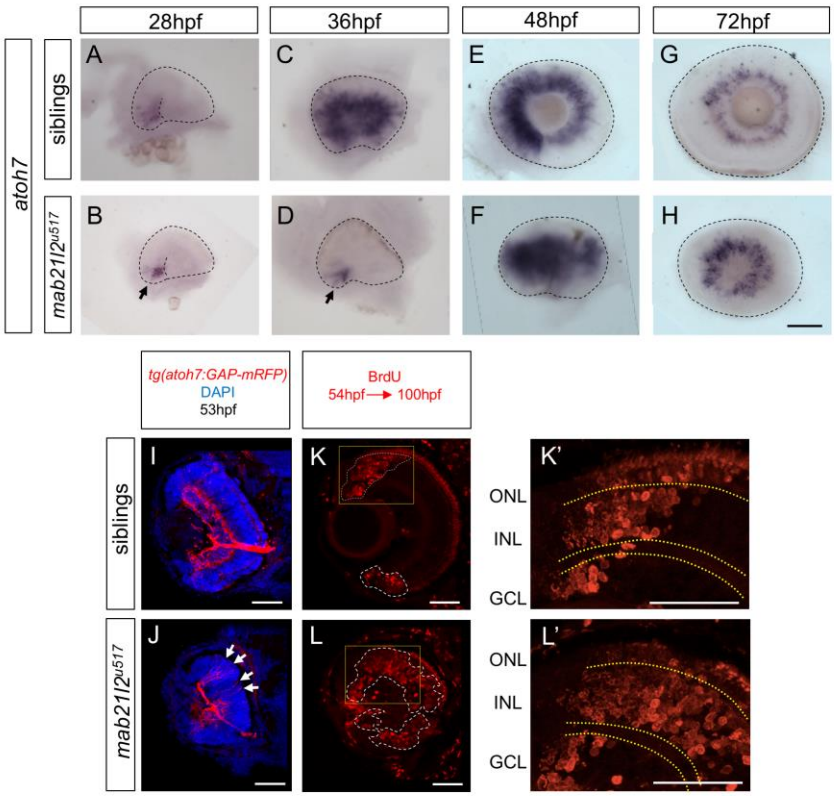

Figure 5. Retinal neurogenesis is delayed in *mab21l2*^{u517} mutants. (A-H) *In situ* hybridization for *atoh7* (purple), a marker for the first neurons to differentiate within the retina. Lateral view of whole mount eyes from sibling and mutant embryos. The dashed line depicts the eye tissue. Black arrows indicate a ventronasal patch of cells of the retina where *atoh7* expression starts. (I, J) Transverse cryosections of retinas stained with DAPI (blue) and RFP (red) and showing nuclei and the expression of *tg(atoh7:GAP-mRFP)*^{cu2}, respectively, at CMZ stages. *mab21l2*^{u517} retinas (J) have a delay in RGC differentiation displaying apical processes, which are features of early neuroepithelial stages (white arrows in J), compared to wildtype (I) at 52hpf. (K-L') Transverse cryosection showing the central layered retina. When a BrdU pulse is given at 54 hpf and chased at 100 hpf, BrdU positive cells (red) in wildtype are found at slightly more central positions but still in the periphery of the retina (K and inset K'). (L and inset L') Mutants display BrdU positive cells in almost the whole eye, suggesting that mutant progenitors keep highly proliferative at CMZ stages (dashed lines). ONL: outer nuclear layer; INL: inner nuclear layer; GCL: ganglion cell layer. Scale bar = 50µm

Supplementary Figure 1

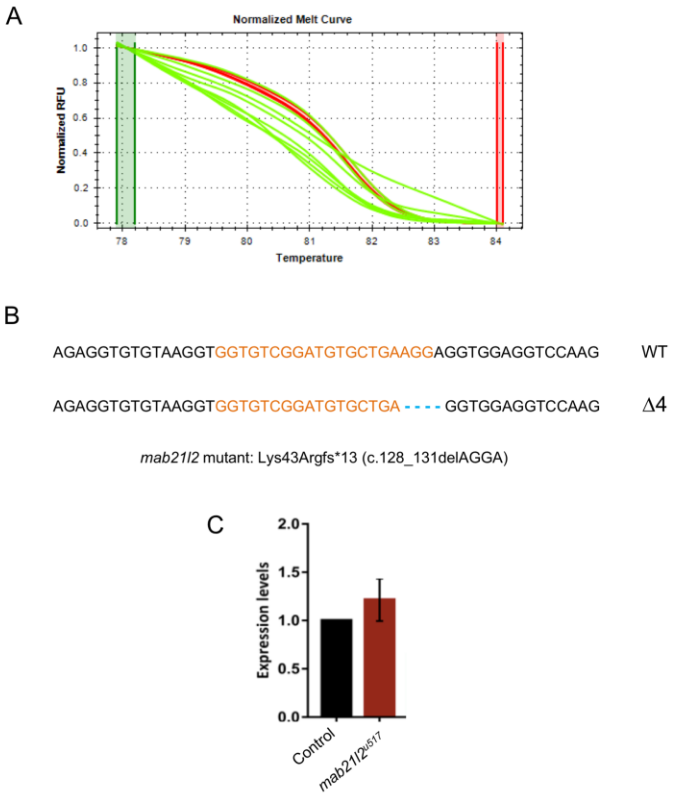

Supplementary figure 1. CRISPR/Cas9 induced mutagenesis of zebrafish *mab21l2* locus. (a) HRMA shows that co-injection of a gRNA targeting the single exon of *mab21l2* and *cas9* mRNA results in somatic mutagenesis in zebrafish embryos at 24 hours post fertilization (F0 generation). Normalized melt curves show differences between uninjected wildtype (red) and injected embryos (green). Green and red boxes at left and right of the graph, respectively, indicate stable pre- and post-melt fluorescence intensity used for normalisation of the data. RFU, relative fluorescence units. (b) The CRISPR/Cas9 induced deletion that was used for characterizing the mutant phenotype. Wildtype (wt) sequence is shown in the top row. gRNA target sequence is highlighted in orange; -, single nucleotide deletion; Δ, number of deleted base-pairs. (C) Quantitative real time PCR for gauging the *mab21l2* mutant transcript levels in 14-somite stages homozygous embryos. Mutants do not display signs of nonsense mediated decay.

Supplementary Figure 2

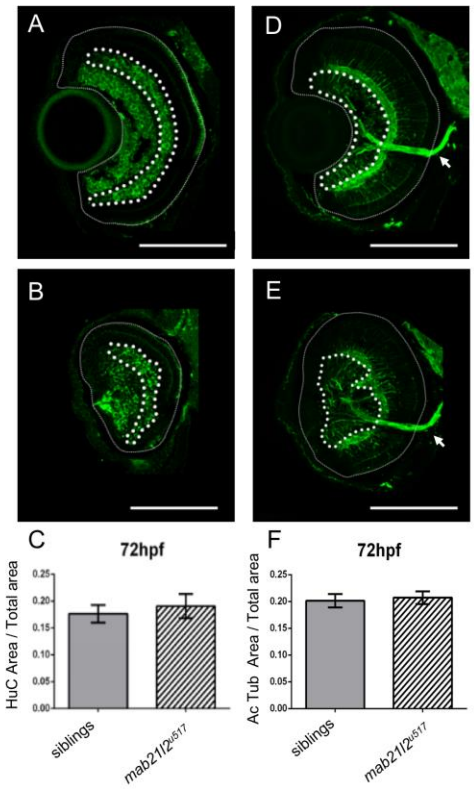

Supplementary figure 2. Cell differentiation does take place in *mab21l2*^{u517}. Images obtained with a confocal microscope of a 72 hpf. (A, C) Immunodetection of HuC/D to identify retinal ganglion cells and amacrine neurons in siblings (A; n=7) and *mab21l2*^{u517} (B; n=7) (labelled in green). (C) The area occupied by amacrine cells over the total area of each section does not change in mutants. (D-F) Immunodetection of Acetylated Tubulin labels neurons and retinal ganglion cells exiting axons (arrows in D and E) within the sibling (n=7) and mutant (n=13) retina. (F) The area occupied by retinal ganglion cells over the total area of each section does not change in mutants. The positive areas from the immunostainings that were used for the graphs in C and F were depicted with dotted line in sibling and mutant retinae in A, B, D and E. (95% confidence limits; Student's t-test; HuC/D p=0.3357; Acetylated tubulin p=0.9048). Scale bar = 100 µm.